Flame response to transverse velocity excitation leading to frequency doubling and modal coupling

Naman Purwar[a,*], Matthias Häringer[a], Bruno Schuermans[b], Wolfgang Polifke[a]

[a]*Technical University of Munich, 85747 Garching, Germany*
[b]*ETH Zürich, 8092 Zürich, Switzerland*

Abstract

Transverse thermoacoustic modes may occur in gas turbines, aero-engines, and rocket engines. Various scenarios of flame excitation can be observed, depending on the type of transverse mode and the location of the flame relative to the mode shape. If an acoustically compact, symmetric flame is exposed to transverse velocity fluctuations of uniform strength and direction, the resulting modulation of the overall heat release rate is invariant to the direction of the velocity perturbation. It follows that the dominant flame response occurs at twice the forcing frequency, even for an infinitesimally small oscillation amplitude. The present study proposes a modeling framework for this inherently non-linear phenomenon, which relies on a second-order kernel of the Volterra series. As a possible realization of the Volterra series, an ad-hoc model is proposed and validated with CFD for mono-frequency forcing. Furthermore, a mechanism of modal interaction is established by which frequency doubling in the flame response causes an unstable transverse mode to drive a higher order stable mode, such that at near-resonance conditions the higher order mode exhibits elevated amplitude. This mechanism can explain the observations made by Urbano et al. [Combustion and Flame 169, 2016] in a small-scale rocket thrust chamber, where a radial mode appears at exactly twice the frequency of the dominant transverse mode. A simple representative setup of a cylindrical combustion

---

[*]Corresponding author
  Email address: `purwar@tfd.mw.tum.de` (Naman Purwar)

chamber is used to explain this mechanism analytically.

1. Introduction

The development of low emission gas turbines, aero-engines, and rocket engines is often thwarted by thermoacoustic instabilities. This type of combustion instability occurs due to a coupling between unsteady combustion and the system acoustics with positive feedback and can cause mechanical failure. Unsteady combustion generates acoustic energy if the heat release fluctuation q' is in phase with the pressure fluctuation p' at the flame. This condition is known as the Rayleigh criterion. One distinguishes between longitudinal and transverse thermoacoustic modes, with acoustic displacement parallel and perpendicular to the direction of the mean flow, respectively. In rocket engines as well as gas turbines, thermoacoustic instabilities are associated frequently with transverse modes [1–8]. Depending on the combustor topology and geometry as well as frequency, transverse modes will appear in a variety of shapes. In combustion chambers with annular or circular cross-sections, amplitudes vary with the azimuthal and/or radial coordinates, whereas in a rectangular chamber, they vary with the principal directions of the cross-section. Generally, a transverse mode can be decomposed into standing and traveling wave components. For the former, there are nodes and anti-nodes of pressure p' and transverse velocity v'. In the following, we will discuss acoustic-flame interactions in terms of standing waves. No essential loss of generality results from this choice, because traveling waves may be represented as superpositions of standing waves and vice versa.

When interacting with transverse modes, flames may be perturbed by axial as well as transverse velocity fluctuations, as reviewed by O'Connor et al. [8]. Figure 1 shows a generic schematic of a flame located at the interface between a burner or injector nozzle and a combustion chamber (c.f. comparable schematics in refs. [8–10]). The flame is assumed to be symmetric about a line (or plane) of

symmetry indicated by the thin, dashed, black line in the figure. This requires that there is no mean transverse flow, but other than that, we make no specific assumptions on the nature of the flame at this point of the discussion. In other words, the figure is to represent in a general manner premixed as well as non-premixed flames with liquid or gaseous fuel.

The precise nature of acoustic-flame interaction depends – among other things – on the position of the flame relative to the mode shape and in particular the (anti-)nodes. Figure 1a depicts a scenario of thermoacoustic interaction – described or modeled, e.g., in refs. [4–8, 11–14] – where pressure oscillation p' in the combustion chamber due to a transverse mode modulates axial velocity u' according to the acoustic impedance of the nozzle, which in turn perturbs the heat release rate q' of the flame. In addition, the flame may be perturbed directly by transverse velocity oscillations v', see for example refs. [9, 15–25] and Fig. 1b. Assuming the flame to be acoustically compact, one concludes that at a pressure anti-node, fluctuations of axial velocity u' and axisymmetric vortical disturbances govern the flame response. Conversely, at a pressure node with $p' = 0$, v' and non-axisymmetric hydrodynamic disturbances dominate. Flames located between anti-nodes of a standing wave or exposed to a traveling wave are subjected to a combination of these types of excitation.

Which one of the two excitation pathways represented by Figs. 1a and 1b is more important and more prevalent in thermoacoustic instability? Heidmann and co-workers [15, 16], e.g., argue that combustion processes in liquid propellant rocket engines, such as atomization and droplet evaporation, are sensitive to both p' and v'. A number of studies focus on the spatial distribution of heat release response of a flame to transverse forcing [17, 20–22, 24, 25]. These investigations are not directly relevant in the present study, which focuses on the global heat release fluctuation of an acoustically compact flame. When limiting the discussion to this scope, the majority of studies agrees that axial velocity perturbation u' dominates the overall flame response [16, 19, 26–28]. On the contrary, transverse velocity fluctuations v', although causing strong flame wrinkling, result only in small modulation of the overall heat release rate q' and

are indeed considered of secondary importance for thermoacoustic instability[1] by many authors [1, 8–10, 15, 19, 29].

Nevertheless, this study is concerned with the flame response to transverse velocity v', as shown in Fig. 1b, with a focus on the intriguing property of *nonlinear frequency doubling* as a result of flame and flow symmetries [15, 30–32]. Fundamentally, this idea may be explained as follows: Excitation by a uniform field of transversal velocity v' is anti-symmetric, because v', being a vector quantity, is anti-symmetric about the center axis of the flame. Figure 2 illustrates reflection symmetry and when a vector field is symmetric and anti-symmetric. Let operator Π be defined for 1D vector field $\overrightarrow{V}$ as $\Pi(\overrightarrow{V}(y)) = -(\overrightarrow{V}(-y))$. This operator performs reflection of $\overrightarrow{V}$ about $y = 0$. The vector field v' is reflection-symmetric if $\Pi(v') = v'$ (Fig. 2 (left)) and reflection-anti-symmetric if $\Pi(v') = -v'$ (Fig. 2 (right)). Thus, a uniform transverse velocity field v' is anti-symmetric at v' anti-node about the center axis of the flame. Here, we focus on flame excitation by this type of v' field. For such an excitation, the flame exhibits invariance to the direction of v', which results in an inherently non-linear dynamics that exhibits frequency doubling in its response to harmonic excitation – even at infinitesimal amplitude!

The phenomenon of frequency doubling as a result of the (anti-)symmetry of flow perturbations and flame, respectively, has been discussed repeatedly in the literature on rocket engines [15, 30, 31, 33], but has been mentioned only once in the literature on gas turbines [32]. This *inherently* non-linear behavior is fundamentally different from the saturation non-linearity related to large amplitude excitation. For the latter, the dominant flame response is at the forcing frequency, while higher harmonics appear with lower amplitudes. For the former, there is no response at the forcing frequency. Instead, the dominant response is at twice the forcing frequency – even for excitation with infinitesimal

---

[1]Cases where the flame is asymmetric, or where large amplitude transverse fluctuations v' change the mean flame shape or interact in a nonlinear fashion with axial velocity fluctuations represent notable exceptions to this general sentiment

4

amplitude.

Let us review previous studies that investigated the flame response to transverse excitation v' with frequency doubling. Heidmann and co-workers [15, 16, 34] explain the phenomenon of frequency doubling in liquid fuel flames as a consequence of the fact that the evaporation rate of fuel droplets is a function of the absolute value of the relative velocity between the gas phase and droplets, and thus invariant to the sign of v'. Zellhuber et al. [32] and Schmid and Sattelmayer [33] showed frequency doubling in the flame response to forcing in transverse direction with unsteady RANS of a premixed swirl flame and a non-premixed flame, respectively, and provided the reasoning of invariant response for it. Given that the response is at a different frequency than the forcing, the aforementioned studies concluded that the unsteady heat release resulting from transversal forcing makes no contribution to the Rayleigh index and thus is insignificant to thermoacoustic stability analysis. Knapp et al. [28, 30] speculated that frequency doubling should occur in LOX/GH2 spray combustion due to direction-invariant coupling of v' with q', and indeed Pomeroy et al. [31], Hardi et al. [35] and Hakim et al. [36] actually observed – or at least gathered indirect evidence for – this phenomenon in experiment and numerical simulations. In other experimental and computational studies of liquid-propellant rocket engine instability, the v' anti-node of the fundamental transverse mode coincides with the p' anti-node of the second order mode in their respective combustion chambers, and thus, the flame is subjected to excitation from both perturbations [12, 37, 38]. Therefore, the flame response at twice the frequency of the fundamental mode may be due to excitation by both transverse velocity and pressure oscillations, making analysis of the flame response difficult.

Complementary to experimental and high-fidelity computational studies, low- or reduced-order models of the flame response to transverse velocity excitation have also been put forward. Crocco et al. [39, 40] proposed a model of q' based on an evaporation rate model, where q' is expressed as an even function of v', such as v'^2, $|v'|$. Sliphorst et al. [41] also used $|v'|$ to formulate a local response factor of q' due to transverse velocity excitation. Ghirardo and

Juniper [42] modeled v' excitation using non-linear functions based on the argument of asymmetric perturbation of the two sides of the flame. However, Harrje and Reardon cautioned in Ch. 4 of ref. [1] against using an even function for phenomena with a symmetric response, since this leads to a discrepancy of the mean heat release with the steady heat release. Acharya et al. [18] and Li et al. [23] used the linearized G-equation to show that the linear response of a symmetric premixed flame to v' is zero. Unfortunately, the response at higher harmonics was not investigated. To summarize, a viable low-order model of the inherently nonlinear flame response to v' excitation has not yet been developed. The present study advocates Volterra series as an adequate modeling framework for this phenomenon, and proposes a first implementation of such a model, which is admittedly ad-hoc and simplistic, but compares favorably with simulation results.

This model is then used to explore modal coupling in a thermoacoustic system with the inherent non-linearity of the flame response to v' excitation. The results suggest that a dominant transverse mode can drive a higher order mode because of frequency doubling in the flame response caused by the v' field of the dominant mode. At near-resonance conditions, i.e., if the eigenfrequency of the higher order mode is close to twice the frequency of the dominant mode, the higher order mode can grow to significant amplitudes. This modal interaction mechanism is structurally different from the established scenarios for non-linear modal interaction, where large amplitude perturbations of the flame leads to unsteady heat release oscillations at higher harmonics, which may couple with a higher order mode, even though the dominant response is at the fundamental frequency [43, 44]. Contrarily, mode coupling due to v' excitation is caused by a flame response with the dominant response at twice the fundamental frequency, and even for infinitesimal small amplitudes. Thus, the present study offers a new perspective to modal interaction caused by the flame response to transversal excitation.

The concepts and models developed are used to develop an alternative explanation of the results of Urbano et al. [45, 46] on thermoacoustic instability

6

in the so-called BKD research combustor, i.e., a small-scale rocket thrust chamber complete with injection manifold and nozzle outlet investigated by Gröning et al. [14, 47–49]. Specifically, Urbano et al. [45, 46] observed in large eddy simulation (LES) of this combustor a strong transverse mode (1T) and simultaneously a radial mode (1R) with considerable amplitude at exactly (!) twice the frequency of the 1T mode. Also, Gröning [49] reports that in experiments, the 1R mode was observed at twice the frequency of the 1T mode with good accuracy. Urbano and Selle [50] provide an explanation of the observed amplitudes of the 1T and 1R modes by quantifying the Rayleigh index and the interaction of acoustics with hydrodynamics. They argue that both modes are unstable, and although the 1T mode has significantly higher Rayleigh index, the 1R mode reaches comparable strength because it has less dissipation than the 1T mode. A low-order model representative of the configuration investigated in refs. [14, 45, 49] is used in this study to demonstrate that the mechanism of modal coupling due to the inherently non-linear flame response to transverse velocity excitation can also explain the aforementioned observation.

The paper is structured as follows: In the next section (Section 2), the non-linear framework for flame response, on which our study is based, is presented and an ad-hoc model based on this framework is proposed for specific applications. CFD simulations of a 2D laminar symmetric flame with v' excitation (c.f. Fig. 1b) are employed to provide direct evidence of the non-linearity and validate the ad-hoc model (Section 3). The proposed ad-hoc model is then applied to model the flame response to v' excitation in a cylindrical combustion chamber (Section 4). Finally, it is shown that the dominant 1T mode drives the 1R mode through transverse excitation at a frequency close to the eigenfrequency of 1R mode, which results in near-resonant amplification. Before proceeding, please note that this paper concentrates on the flame response to a uniform v' only (shown in Fig. 1b). For the sake of brevity, "flame response" will be used in place of "flame response to uniform v'", unless explicitly stated.

2. Non-linear model for flame response (compact flame)

When a flame is excited by transverse velocity perturbation, it responds with fluctuation in heat release rate. The flame response involves many complex physical processes, which depend on the flame type, e.g., premixed, non-premixed, or partially premixed flame, or the flame stabilization mechanism, i.e., bluff body, or swirl, etc. Other processes, like evaporation, droplet breakup, occur in combustion of liquid fuel. As mentioned in the Introduction, the flame response is invariant to the direction of v' irrespective of the type of flame. Therefore, we seek to develop a lumped low-order model describing the dynamics of the global response of the flame instead of developing detailed models for individual processes. Apart from the flame being acoustically compact and symmetric, it is important that for both excited and unexcited flame, there is a complete consumption of fuel or oxidizer before the flow exits the confinement. To this end, we treat the flame as a dynamical system and introduce a framework based on Volterra series, which appears suitable for modeling the inherent non-linearity (the invariant behavior) of the flame response.

In a linear time-invariant (LTI) dynamic system, output $y(t)$ and input can be linked by convolution of the input $u(t)$ and its unit impulse response $h(t)$ [51]:

$$y(t) = \int_0^t h(\tau)u(t-\tau)d\tau \tag{1}$$

Such system allows superposition and exhibits linear scaling properties. As a generalization of (1), input and output of a Non-linear Time Invariant (NLTI) system can be related using Volterra series [51, 52]:

$$
\begin{aligned}
y(t) = &\int_0^t h_1(\tau)u(t-\tau)d\tau \\
&+ \int_0^t \int_0^t h_2(\tau_1,\tau_2)u(t-\tau_1)u(t-\tau_2)d\tau_1 d\tau_2 + ... \\
&+ \int_0^t ... \int_0^t h_n(\tau_1,...,\tau_n)u(t-\tau_1)...u(t-\tau_n)d\tau_1...d\tau_n
\end{aligned}
\tag{2}
$$

where the nth-order Volterra kernel h_n is real.

Let us formulate the invariant behavior of heat release fluctuation to the direction of v' in mathematical terms. Denoting the convolution-operation in Eq. (2) as $q'(t) = H(v'(t))$, the property of invariance to the direction of v' says:

$$H(v'(t)) = H(-v'(t)) \tag{3}$$

Equation (3) holds for arbitrary v'. Applying this property to Eq. (2), the even Volterra kernels on the left and the right hand side of Eq. (3) cancel, leaving only the odd Volterra kernels:

$$
\begin{aligned}
\int_0^t .. \int_0^t h_n(\tau_1, .., \tau_n)v'(t - \tau_1)..v'(t - \tau_n)d\tau_1..d\tau_n = \\
- \int_0^t .. \int_0^t h_n(\tau_1, .., \tau_n)v'(t - \tau_1)..v'(t - \tau_n)d\tau_1..d\tau_n
\end{aligned}
\tag{4}
$$

where n is an odd number. If Eq. (4) is to hold for any input v', h_n is identically zero when n is an odd number. It follows that the Volterra series of $q'(t)$ comprises of only even-order kernels. The second-order kernel is the leading term and is expected to dominate the response for small v'. Hereon, we will restrict our consideration to the second-order kernel for modeling the flame response as in Eq. (5).

$$q'(t) = \int_0^t \int_0^t h_2(\tau_1, \tau_2)v'(t - \tau_1)v'(t - \tau_2)d\tau_1 d\tau_2 \tag{5}$$

2.1. Frequency domain response of 2nd order NLTI system

When an NLTI system as defined in (5) is excited with mono-frequency harmonic input, its output will in general be a combination of a constant offset and a harmonic component at twice the input frequency. This can be shown as follows: Substituting $v'(t) = A\cos\omega t = A(e^{i\omega t} + e^{-i\omega t})/2$ in Eq. (5), one obtains (details of the derivation are given in the Appendix provided as Supplemental material):

$$q'(t) = \frac{A^2}{2}\Re[e^{2i\omega t}\psi(\omega, \omega) + \psi(\omega, -\omega)] \tag{6}$$

with a second order transfer function ψ derived as:

$$\psi(\pm\omega_1, \pm\omega_2) \equiv \int_0^t \int_0^t h_2(\tau_1, \tau_2)e^{\mp i\omega_1\tau_1}e^{\mp i\omega_2\tau_2}d\tau_1 d\tau_2 \tag{7}$$

The first term in angular brackets on the r.h.s. of Eq. (6) represents an output component that oscillates at frequency 2ω, i.e., twice the frequency of the input. Gain and phase of the response at that frequency is governed by the second order transfer function ψ. The second term in angular brackets $\psi(\omega, -\omega)$ is time-independent, i.e., it represents a constant offset. However, transverse excitation does not change the amount of fuel or oxidizer consumed in combustion (if one excludes events such as incomplete consumption of fuel/oxidizer, or even extinction due to very large amplitudes). It follows from fundamental conservation laws that the mean heat release rate for a transversaly forced flame must not deviate from its steady-state value (c.f. arguments given in ref. [53] for the low frequency limit of flame transfer functions). Hence $\psi(\omega, -\omega) = 0$ in the present case – a conclusion that will be confirmed by numerical results in Section 3.

Note that a second order transfer function has two frequencies as input variables. To understand the importance of these two frequencies, we first recapitulate the concept of transfer function. In an LTI system, the output is at the same frequency as the input. Thus, the output can be linked to the input through a transfer function in frequency domain and harmonic probing with mono-frequency input provides quantitative information on the transfer function in an LTI system. Contrarily, in a purely second order system, like the one studied here, one must use two independent frequencies in harmonic probing to obtain full knowledge of the second order transfer function (ψ). Thus, ψ varies over a 2D plane of frequencies (Fig. 3). Harmonic probing with single frequency gives the variation of ψ only along the diagonal $\omega_1 = \omega_2$. This plot is symmetric with respect to $\omega_1 = \omega_2$ line. At the $\omega_1 = -\omega_2$ line, ψ should be zero, as there should be no bias in the output.

2.2. Time Domain ad-hoc model

As described in Eq. (5), the flame response can be represented in the time domain by a second-order convolution integral. Thus, if we know or are able to obtain the h_2 kernel, we can compute the time domain response for any input

signal. In this study, we do not aim to identify this kernel because its quantitative properties would be case dependent. Instead, we propose an ad-hoc model, which has minimal properties of the h_2 kernel and can be used for a specific type of input signal. Here, we focus only on mono-frequency harmonic input signals. This ad-hoc model can be substituted for the complete h_2 kernel for qualitative analysis in time-domain low-order modeling. This model is applied in Section 4 to demonstrate its convenient behavior. The ad-hoc model for single frequency forcing is presented as follows:

$$q'(t) = kv'(t - \tau)\frac{dv'(t - \tau)}{dt} \tag{8}$$

where, k is a coefficient corresponding to the gain and τ is an overall time delay. It should be noted that we do not provide theoretically derived values for k and τ, and their values must be set to match the actual levels of q' from the flame as will be demonstrated in Section 3. Thus, k and τ are parameters which are expected to vary with forcing frequency. It can be noted that the presented ad-hoc model is similar to the commonly used $n-\tau$ model of Crocco and Cheng [54] as both require two parameters which need to be determined from the actual response of the flame. However, the $n - \tau$ model is used to model linear flame response, whereas Eq. 8 can model a second order flame response.

Here we give a brief argument to demonstrate that this ad-hoc model (Eq. (8)) is a suitable candidate for the flame response. The ad-hoc model needs to satisfy two conditions:

(i) it should be possible to represent this model in terms of the second-order kernel of the Volterra series as in Eq. (5).

(ii) the model output should have a zero offset because the mean heat release of the flame with excitation remains unchanged.

To satisfy the first condition, we assume a functional form of h_2 kernel, which when substituted in Eq. (5) results in Eq. (8). Let us assume h_2 kernel as:

$$h_2(\tau_1, \tau_2) = \frac{k}{d\tau}[\delta(\tau_1 - \tau)\delta(\tau_2 - \tau) - \delta(\tau_1 - \tau)\delta(\tau_2 - \tau - d\tau)] \tag{9}$$

11

where, $\delta(t)$ is a delta function. Substituting this kernel in Eq. (5), integrating over $d\tau_1$ and $d\tau_2$ and replacing $d\tau$ with dt, we get in the limit of infinitesimal dt:

$$
\begin{aligned}
q'(t) &= \lim_{dt \to 0} \frac{k}{dt} [v'(t-\tau)\, v'(t-\tau) - v'(t-\tau)\, v'(t-\tau-dt)] \\
&= k\, v'(t-\tau) \lim_{dt \to 0} \frac{v'(t-\tau) - v'(t-\tau-dt)}{dt} \\
&= k\, v'(t-\tau) \frac{d(v'(t-\tau))}{dt}
\end{aligned}
\tag{10}
$$

This shows that the proposed ad-hoc model is one possible realization of the Volterra series. Please note that the chosen h_2 kernel is valid only for a mono-frequency input. To examine the second requirement, we give a harmonic input $(v'(t) = A \cos \omega_0 t)$ to this model and get:

$$
q'(t) = k\frac{A^2}{4}\Re[i\omega_0(e^{2i\omega_0(t-\tau)} - e^{-2i\omega_0(t-\tau)})] = -k\frac{A^2}{2}\omega_0 \sin 2\omega_0(t-\tau) \tag{11}
$$

It is evident that the model gives an output oscillating at frequency $2\omega_0$. Moreover, there is no constant bias. Here, we emphasize this important feature because a constant offset is present in the models for the flame response proposed previously by Crocco et al. [39, 40], which were based on using symmetric functions, like v'^2 or $|v'|$. Such a symmetric function changes the mean heat release [1], whereas the proposed ad-hoc model does not suffer from this shortcoming.

It can be noted that the term $v'(t-\tau)\, d(v'(t-\tau))/dt$ in Eq. (8) has an undesirable feature as it increases without bounds for higher frequencies of v'. However, the term k can compensate as it is a parameter that can vary with the forcing frequency and lead to physical values of q'. In the absence of the actual q' from the flame response, k can be chosen such that it exhibits low-pass filter behavior for modeling the flame response over a wide frequency range to avoid divergent response at high frequencies. It is demonstrated in Section 3 that this model can give quantitative agreement for mono-frequency input. This ad-hoc model can be added to the model of flame response to axial excitation to perform low-order modeling of transverse modes. An application of this model is discussed in Section 4. The combined model in the application has the axial

12

excitation model based on Noiray et al. [55] and Bonciolini [56] and takes the following form:

$$q'_{ax+trans}(t) = nu'(t - \tau_{ax}) - \mu u'^3(t - \tau_{ax}) + kv'(t - \tau)\frac{dv'(t - \tau)}{dt} \qquad (12)$$

where, the first term gives the time delayed linear response to axial velocity perturbation u', the second term corresponds to the saturation non-linearity due to u' and the third term comes from the ad-hoc model for v' excitation. The results of ref. [16, 32, 33] are reiterated here again that q' due to v', being at twice the frequency of the excitation, cannot lead to self-excited instability. However, it can cause modal coupling and near-resonance amplification of amplitudes of other modes (demonstrated in Section 4).

3. CFD simulation with v' excitation

In this section, the results of the theoretical analysis in Section 2 are confirmed by the means of CFD. We study the response of a 2D laminar premixed slit flame subjected to v' forcing as indicated in Fig. 4. While the considered generic configuration is computationally inexpensive, we expect it to contain all the features relevant in the present context. The results from other studies, like refs. [32, 33, 36], suggest that more applied configurations, like turbulent or non-premixed flames, show qualitatively the same behavior.

The present setup is inspired by the laminar slit burner from ref. [57]. This configuration was simulated with CFD in numerous previous studies, for example, refs. [58, 59], although not in the context of transverse excitation. Nevertheless, the numerical setup used in these studies is very similar to the present one.

The solver employed here is a customary low Mach number formulation of the *rhoReactingFoam* solver from the open-source package OpenFOAM, which was also used in ref. [58]. In this *weakly compressible* approach, where the density depends only on temperature but not on pressure, acoustic waves do not exist. This simplification is valid here, because the flame is acoustically

13

compact, with its length and width being much smaller than the acoustic wavelengths considered. The advantage of this formulation is that the transverse forcing does not excite axial perturbations, as it would be the case in a fully compressible setup like in ref. [60]. The flame response to v' excitation can thus be studied independently from any axial excitation.

The solver settings, spatial and temporal schemes and the two-step chemistry model of methane-air combustion are identical to those used in ref. [58]. The mesh is uniform and orthogonal with a cell size of 25 μm corresponding to 18 grid points in the reactive zone. The time step is set to $\delta t = 5e^{-7}$ s resulting in a Courant number well below 0.1.

At the inlet, Dirichlet-type boundary conditions are set for flow velocity, species mass fractions and temperature, while a Neumann-type condition (zero gradient) is set for pressure. At the outlet, the pressure is fixed at 10^5 Pa (Dirichlet-type), while a zero gradient condition is imposed for all other variables. The inlet temperature is 293 K and the equivalence ratio is 0.8. A constant velocity profile with an area weighted mean value of 1 m/s is imposed at the inlet. The flame is anchored at an adiabatic non-slip plate (see Fig. 4).

At the boundaries on the left and right side of the flame the steady axial mean velocity is superposed with a mono-frequent velocity forcing in transverse direction (Fig. 4). The normalized (global) heat release fluctuation

$$q'(t) = \frac{q(t) - \overline{q}}{\overline{q}} \tag{13}$$

is obtained by subtracting the steady state heat release rate $\overline{q}$ from the instantaneous $q(t)$.

Figures 5 and 6 show the resulting q' for a mono-frequent transverse forcing at $f = 400$Hz. Figure 5 shows that the output is seen only at twice the frequency of the input thus providing the evidence of q' being invariant to the direction of transverse velocity v' (refer to Section 2). The output at the forcing frequency is negligible. There is no offset in the response as there is no discernible amplitude at 0 Hz, confirming the statement made in Section 2.1 regarding the constant term in Eq. (6) to be equal to 0. Figure 6 depicts that q' scales with the square

14

of amplitude of the input as predicted in Eq. (6). In addition to this, the ad-hoc model, proposed in Section 2.2, is able to reproduce the output of CFD in time-domain (Fig. 6). The parameters k and τ are obtained by minimizing the error between CFD and the ad-hoc model output. It is important to note that in the case simulated here, k and τ do not vary with amplitudes (even up to a forcing amplitude of 50% of the axial mean flow), but only with frequency. However, it is possible in other cases that at higher amplitudes, when other higher order even kernels become significant, k and τ might vary with amplitude as this ad-hoc model can only model the second order response. Although the normalized q' is very small compared to the normalized v' for the simulated flame setup, it can be significantly higher for other flame setups (for example Zellhuber et al. [32]).

4. Application to thermoacoustic instability in a research combustor

In the previous sections, we have proposed a simple low-order model to capture the inherent non-linearity in flame response to excitation by transverse velocity v'. As suggested in other studies, this response is generally weaker than the flame response to axial velocity perturbations. However, the oscillation of heat release rate q' caused by v' can result in coupling of a transverse mode to another higher order mode at twice the frequency. The resulting oscillation amplitudes will depend on the closeness of the eigenfrequencies of higher order modes to the frequency of excitation by q' oscillation: if the eigenfrequency of a higher order mode is close to twice the eigenfrequency of the fundamental transverse mode, significant amplitudes may be achieved due to (near-)resonant amplification – even if the flame response to v' as such is weak. The relevant thermoacoustic interaction mechanisms of this scenario are depicted in Fig. 7. Häringer et al. [43] demonstrated a comparable phenomenon in a longitudinal combustor with a laminar flame, where the second harmonic of a linearly unstable mode at large oscillation amplitude causes resonance with another acoustic mode, resulting in higher amplitude for the latter compared to the unstable

mode.

We shall demonstrate in the following that a stable radial mode in a cylindrical combustion chamber may be forced by an unstable transverse mode. This mechanism of modal coupling is then put forward as a possible explanation of the observation of frequency-doubled modes made by Urbano et al. [45] and Gröning [49]. We briefly discuss these observations here.

Gröning [14, 47–49] conducted experiments on a small-scale rocket thrust chamber designated as BKD combustor. This setup included injection domes, injectors, a combustion chamber, and a nozzle outlet. Urbano et al. [45] carried out a Large-Eddy Simulation (LES) of this configuration and ascertained that power spectral densities (PSD) obtained from the LES show good agreement with the experiments. In particular, the PSD of pressure fluctuations from the LES (reproduced in Fig. 8) shows two peaks at frequencies $f_1 = 10,700 Hz$ and $f_2 = 21,400 Hz$, which correspond to transverse (1T) and radial (1R) modes, respectively, according to the spatial structure of the perturbations. Corresponding peaks in the experimental time series data are observed at 10,260 Hz and 20,500 Hz [45]. This is confirmed by Gröning [49], who commented that "with good accuracy" the 1R mode is at twice the frequency of the 1T mode.

In a subsequent study, Urbano et al. [46] argue – in line with Gröning et al. [14] – that the heat release oscillation at f_1 is predominantly driven by axial velocity perturbations u' at the fuel injector exit, which in turn are induced by pressure fluctuations p' of the 1T mode.

To substantiate this argument, Urbano and Selle [50] quantified the Rayleigh index and the interaction of acoustics with hydrodynamics for both modes. For both modes, the Rayleigh index is positive, and it is concluded that both modes are unstable. The Rayleigh index of the 1R mode is significantly lower than that of the 1T mode, but the comparatively lower dissipation of the 1R mode can account for the fact that the amplitude of this mode is nevertheless considerable.

In the current study, we put forward an alternative explanation to the observation of significant amplitude of the 1R mode on the basis of frequency doubling in the flame response due to v' excitation. In this context, it is im-

portant that the observed frequency of the 1R mode (f_{1R}) is exactly twice the frequency of the dominant 1T mode (f_{1T}) in the LES results [45] and within 0.1% in the experimental results [49]. This observation is relevant because the acoustic eigenfrequency of the 1R mode ($f_{1R,eigen}$) is not necessarily exactly equal to twice the eigenfrequency of the 1T mode ($f_{1T,eigen}$). One can show analytically (see Section 4.1) that for a cylindrical chamber $f_{1R,eigen}$ is close to $2f_{1T,eigen}$ (within 4.05% from $2f_{1T,eigen}$, to be precise), but not exactly equal. Similarly, Schulze and Sattelmayer [61] computed via 3D numerical solution of the linearized Euler equations the eigenfrequencies of the 1T and 1R modes of the BKD setup for non-reacting mean flow conditions to find that $f_{1R,eigen}$ lies close to $2f_{1T,eigen}$ (within 3.7 %). Finally, Urbano et al. [45] computed the eigenfrequencies of the 1T and 1R modes in the BKD setup (but without the hydrogen dome and with equivalent impedances in place of the hydrogen stream and the nozzle outlet) with a Helmholtz solver. It was observed that the eigenfrequencies are quite sensitive to the spatial distribution of the speed of sound, and exact equality between the eigenfrequencies $f_{1R,eigen}$ and $2f_{1T,eigen}$ was found for a particular spatial distribution of the speed of sound.

To conclude, while it can be said with confidence that $f_{1R,eigen}$ is close to $2f_{1T,eigen}$, exact equality should be considered to be a mere coincidence, if one regards the observed oscillation frequencies as eigenfrequencies of two uncoupled, unstable modes. Conversely, if one argues that there is mode coupling with frequency doubling, such that the 1R mode is driven at near-resonance conditions by the unstable 1T mode (see Fig. 7), the oscillation frequencies *must* obey the relation $f_{1R} = 2f_{1T,eigen}$.

To provide further support for this scenario of modal coupling with near-resonant driving of the 1R mode, we apply the model developed for v' excitation in the above sections to a rocket thrust chamber represented by a cylindrical chamber. We make some assumptions based on conclusions from previous studies to make our analytical explanation simpler. From a study on cumulated Rayleigh index along the axial direction, Urbano et al. [45] conclude that it might be possible to assume the flame to be acoustically compact even though

17

the frequencies of the modes are above 10kHz. This conclusion is important for our explanation, because the model of flame response to v' is valid for compact flames. We reduce the order of model by considering only the early flame region (Fig. 9) because this region drives the combustion instability [45]. Thus, we neglect the longitudinal distribution of the acoustic variables in the combustion chamber and injectors. Although it has been shown in refs. [14, 45, 46] that injectors play an important role in determining the stability and the oscillation amplitude of the 1T mode, we do not include the acoustics of the injectors in our analysis because we consider it to be given that the 1T mode is dominant and unstable. Instead, we focus on the dynamics of the 1R mode and including injectors in our analysis is not essential for the proposed mode coupling mechanism. It is only essential that $f_{1R,eigen}$ is close to $2f_{1T,eigen}$.[2] It is shown later in Section 4.1 that this condition is satisfied even without injectors and the longitudinal extension of the chamber. We also assume a homogeneous field of speed of sound and no mean flow in the chamber for the reason mentioned previously. Thus, the acoustic modes in the combustion chamber are confined to the early flame region and depend spatially only on r and θ.

Harrje and Reardon in Ch. 4 of ref. [1] provide extensive information about modeling acoustic modes in rocket engines. We use a simplified model to show mode coupling. In the BKD setup, injectors are placed axisymmetrically around the center axis of the chamber with three concentric rings. Similarly, we assume that the distribution of acoustic sources (flames) in our model is axisymmetric around the center axis of the cylindrical chamber and also uniform in both circumferential and radial directions. The assumption of uniform distribution of flames does not affect our explanation to the observations in ref. [45], which will be detailed later in Section 4.1. Flames are assumed to respond to axial velocity perturbation induced by p' (based on the conclusions from Urbano et

---

[2]This mechanism of modal coupling is not possible for 2T and 3T modes because $f_{2T,eigen}$ and $f_{3T,eigen}$ are not close to $2f_{1T,eigen}$. Schmid and Sattelmayer [33] provide the same argument, but they do not consider the possiblity of coupling with the 1R mode.

al. [46]) and v' perturbations. The modeling of flame response is done with the lumped low-order model presented in Eq. 12. We reiterate here that we do not analyse the stability of the 1T mode and assume it to be given that it is dominant and unstable. We rather focus on the dynamics of the 1R mode.

4.1. Oscillator model

First, the oscillator model for a cylindrical combustion chamber with no mean flow and homogeneous field of speed of sound is derived from the acoustic wave equation with unsteady heat source term :

$$\frac{\partial^2 p'}{\partial t^2} - c^2 \nabla^2 p' = (\gamma - 1)\frac{\partial q'}{\partial t} \tag{14}$$

where,

$$\nabla^2 p' = \frac{1}{r}\frac{\partial}{\partial r}(r\frac{\partial p'}{\partial r}) + \frac{1}{r^2}\frac{\partial^2 p'}{\partial \theta^2}. \tag{15}$$

Please note that all partial derivatives with respect to the longitudinal direction are neglected. p' is expressed in complex terms as $\hat{p}'(r,\theta)e^{i\omega t}$. Similarly, v'_r and v'_θ (velocity in radial and azimuthal direction, respectively) can also be expressed in terms of complex amplitudes. Solution of these complex amplitudes for purely transverse modes are given as in ref. [1]:

$$
\begin{aligned}
\hat{p}'(r,\theta) &= P\psi_{\nu\eta}(r)e^{i\nu\theta} + ... \\
\hat{v}'_r(r,\theta) &= V_r\frac{d\psi_{\nu,\eta}(r)}{dr}e^{i\nu\theta} + ... \\
\hat{v}'_\theta(r,\theta) &= V_\theta\frac{\psi_{\nu,\eta}(r)}{r}e^{i\nu\theta} + ...
\end{aligned}
\tag{16}
$$

where $\psi_{\nu\eta}(r) = J_\nu(s_{\nu\eta}r)$ is described by a Bessel function of the first kind.

The value of $s_{\nu\eta}$ is obtained by applying the boundary conditions. Here, we assume a solid wall at $r = R$. Hence, $\hat{v}'_r(r = R) = dJ_\nu(s_{\nu\eta}r)/dr|_{r=R} = 0$. As we are interested only in the 1T and 1R modes, we get $s_{1,1}R = s_{1T}R = 1.8413$ and $s_{0,2}R = s_{1R}R = 3.8317$. This gives the ratio $f_{1R,eigen} = 2.081f_{1T,eigen}$. Therefore, the eigenfrequency of the 1R mode is close to twice the eigenfrequency of the 1T mode. Here, we only consider standing modes because Urbano et al. [45] also observed a standing 1T mode in their simulation. However, the model

can be easily extended to rotating modes. Now, with the values of $s_{1,1}$ and $s_{0,2}$ known, p' can be written as:

$$p'(r, \theta, t) = \Re[A_1 J_1(s_{1T}r) \cos \theta e^{i\omega_{1T}t} + A_2 J_0(s_{1R}r)e^{i\omega_{1R}t}]$$
$$= \eta_1(t)J_1(s_{1T}r) \cos \theta + \eta_2(t)J_0(s_{1R}r) \tag{17}$$

Figures 10c and 10d show the spatial distributions of pressure fluctuations p' of the 1T and 1R mode according to Eq. (17). Figure 10e shows the transversal velocity v' of the 1T mode according to Eq. (16). It is evident that the spatial distribution of $\hat{v}'$ of the 1T mode (v'_{1T}) and $\hat{p}'$ of the 1R mode (p'_{1R}) have common features: the v' anti-nodal line passes through the center of the chamber and coincides with the p' anti-node of the 1R mode. As v'_{1T} leads to q' at twice the frequency, which is close to $f_{1R,eigen}$, near-resonance thermoacoustic driving of the 1R mode may occur. This resonance is expected to be strong because the region of maximum amplitude of q' driven by v'_{1T} coincides with the p' anti-node of the 1R mode. This hypothesis is supported by the distributions of q' from ref. [46], which are reproduced in Figs. 10a and 10b. Figs. 10a and 10c clearly show that for the 1T mode, the maximum amplitude regions of q' and p' distributions coincide. For the 1R mode, Fig. 10b shows that the center of the chamber has the maximum amplitude for q', which is also the region of maximum amplitude for both v'_{1T} and p'_{1R} (Fig. 10e and 10d). In summary, we can state that the spatial distributions of fluctuations of pressure, velocity and heat release rate support the hypothesis of near-resonance thermoacoustic driving of the 1R mode.

Another important question is whether the positive Rayleigh index observed by Urbano et al. [50] for the 1R mode necessitates indeed that this mode is unstable and conversely rules out the possibility that the 1R mode is driven by the frequency-doubled heat release fluctuations that originate with the 1T mode? In general, the answer to this question is negative! Consider a mode that is linearly stable against self-excited fluctuations, because the Rayleigh index that results from acoustic-flame feedback is negative or not large enough to overcome acoustic dissipation. If such a mode is forced by externally imposed unsteady

heat release to oscillate with some finite amplitude, the thermoacoustic interactions between unsteady heat release and pressure must provide the acoustic energy that is consumed by dissipation. In other words, the Rayleigh index that is observed in this case must be positive, even though without external thermoacoustic driving a negative Rayleigh index would be observed. In complete agreement with this general argument, we show below that the Rayleigh index predicted with the oscillator model of the BKD developed in this section is indeed positive at near-resonance.

Close observation of Fig. 10b brings further insight. It can be noticed that the spatial distribution of q' of the 1R mode (Fig. 10b) is elliptical with the major axis along the p'_{1T} nodal line (corresponding to the region with $q' \approx 0$ in Fig. 10a). This indicates that the spatial distribution of total q' at frequency f_{1R} is a superposition of q' from axial velocity oscillation induced by p'_{1R} (Fig. 10d) and q' from v'_{1T} (Fig. 10e). Expressing this mathematically, $q'_{f_{1R}} = q'_{axial,1R} + q'_{trans,1T}$. Therefore, $q'_{trans,1T}$ cannot be ignored if it is significant in comparison to $q'_{axial,1R}$. Same observation was made in refs. [12, 37, 38], where the v' anti-node of the fundamental mode coincided with the p' anti-node of the second order mode, suggesting that the flame responds to both perturbations. Due to this superposition, a positive Rayleigh index computed with $q'_{f_{1R}}$ and p'_{1R} does not indicate that q' provides a constructive feedback to the 1R mode causing instability because $q'_{f_{1R}}$ contains $q'_{trans,1T}$, which is forcing by another mode. If the stability of the 1R mode is to be determined, a Rayleigh index computed with $q'_{axial,1R}$ should be compared with the damping. However, $q'_{axial,1R}$ and $q'_{trans,1T}$ are at the same frequency and thus, decomposition of $q'_{f_{1R}}$ in these two components is not straightforward. This results in two possibilities: (1) the 1R mode is unstable and reaches a limit cycle at high amplitudes even without decisive influence of $q'_{trans,1T}$; (2) the 1R mode is stable and forced by $q'_{trans,1T}$ at near-resonance conditions. The available data do not allow to rule out any one of the two scenarios with confidence. In the following, we explore the second possibility with an analytical model and elucidate in more detail the mechanism of the 1T mode forcing the 1R mode through frequency-doubled flame response.

Recall Fig. 7, which shows a schematic of the modal coupling between an unstable transverse mode and a stable higher order mode through v' excitation. As mentioned earlier, pressure oscillation p' of the 1T mode induces axial velocity oscillation at the injector exit u'_{inj} according to the acoustic impedance at the injector exit Z_{inj}. Heat release rate fluctuations q' driven by this velocity oscillation may provide constructive feedback [46]. Indeed, we consider the 1T mode to be linearly unstable (the unstable transverse mode in Fig. 7). On the contrary, according to the mechanism proposed in this study, the 1R mode is forced by q' due to v'_{1T}. Thus, even if the 1R mode is linearly stable, forcing close to the eigenfrequency of the 1R mode will lead to high amplitude of this mode. To explore this possibility, we consider the 1R mode to be stable (the stable higher order mode in Fig. 7). In the following, we simplify the oscillator models for the 1T and 1R modes separately after modeling the source terms in the acoustic wave equation.

Let us first write separate wave equations for the oscillator variables of the 1T and 1R modes (η_1 and η_2 respectively) without source terms :

$$J_1(s_{1T}r)\ddot{\eta}_1 - c^2 \left[\frac{1}{r}\frac{dJ_1(s_{1T}r)}{dr} + \frac{d^2 J_1(s_{1T}r)}{dr^2} - \frac{J_1(s_{1T}r)}{r^2} \right]\eta_1 = 0 \qquad (18)$$

$$J_0(s_{1R}r)\ddot{\eta}_2 - c^2 \left[\frac{1}{r}\frac{dJ_0(s_{1R}r)}{dr} + \frac{d^2 J_0(s_{1R}r)}{dr^2} \right]\eta_2 = 0 \qquad (19)$$

Unstable 1T mode :

For linear analysis, q' due to u' can be modeled in terms of η_1 with a gain G and a time delay τ_l [54, 55]. Assuming a uniform distribution of heat sources in the combustion chamber, $\partial q'/\partial t$ can be added to the right side of Eq. (18). The resulting equation can be multiplied with r^2 and integrated from 0 to R. After rearrangement and renaming of the constants, it can be reduced to:

$$\ddot{\eta}_1 + \alpha_1 \dot{\eta}_1 + \omega_1^2 \eta_1 = \beta_1 \dot{\eta}_{1,\tau_l} \qquad (20)$$

where, α_1 is added to account for damping. It should be noted that in our analytical model, flames are assumed to be distributed uniformly in radial and azimuthal direction. However, in the BKD setup, injectors are placed within three concentric rings and at discrete uniform azimuthal intervals, which makes the distribution axisymmetric about the center of the chamber. The integration performed to obtain Eq. 20 with a discrete axisymmetric distribution of flames only affects the coefficient on the right side of Eq. 20 and does not change the dynamics of this mode qualitatively. Therefore, our assumption of uniform distribution of flames is valid. Saturation of the flame response at high amplitudes is taken into account with following modification as in ref. [56]:

$$\ddot{\eta}_1 + \alpha_1 \dot{\eta}_1 + \omega_1^2 \eta_1 = (\beta_1 - \kappa_1 \eta_{1,\tau_l}^2)\dot{\eta}_{1,\tau_l} \tag{21}$$

where, κ_1 is the coefficient of the cubic saturation non-linearity. One can also derive the right side of Eq. 21 using the model of flame response to axial excitation from the first two terms on the right side in Eq. 12. As the 1T mode is linearly unstable, $\beta_1 > \alpha_1$ and any other type of forcing is neglected. For demonstration, let us assume $\tau_l = 0$. Limit cycle amplitude and frequency for the 1T mode is calculated as in ref. [56]:

$$A_{1,lc} = 2\sqrt{\frac{\beta_1 - \alpha_1}{\kappa_1}} \tag{22}$$

and

$$\omega_{1,lc} = \omega_1 \tag{23}$$

Stable 1R mode :

A similar approach can be applied to the 1R mode to simplify the oscillator model for η_2 (Eq. (24)). As the 1R mode is stable, $\beta_2 < \alpha_2$. Thus, external forcing plays a dominant role which is also added in the oscillator model. It should be noted that the saturation non-linearity term from the axial excitation

is dropped as this oscillator is linearly stable with respect to axial excitation.

$$\ddot{\eta}_2 + \alpha_2 \dot{\eta}_2 + \omega_2^2 \eta_2 = \beta_2 \dot{\eta}_{2,\tau_l} + F \tag{24}$$

Now, we need to model F. As mentioned earlier, this external forcing originates from q' at frequency $2\omega_1$ due to v'_{1T}. The spatial distribution of v'_{1T} can be derived from Eq. (16).

$$v'(r,\theta,t) = v'_r \hat{e}_r + v'_\theta \hat{e}_\theta = \chi_1(t)\phi(r,\theta) \tag{25}$$

where, $\dot{\chi}_1(t) = \eta_1(t)$. q' due to v'_{1T} is modelled according to the ad-hoc model proposed in Section 2.2. Substituting v' from Eq. (25) in Eq. (8) leads to:

$$q'(t,r,\theta) = k\phi^2(r,\theta)\chi_1(t-\tau)\dot{\chi}_1(t-\tau) = k\phi^2(r,\theta)\chi_1(t-\tau)\eta_1(t-\tau) \tag{26}$$

Again, for demonstration purpose, τ is taken to be 0 in Eq. 26 and $\tau_l = 0$ in Eq. 24. In order to apply this source term in the oscillator model, we need to add $\partial q'/\partial t$ from Eq. (26) in Eq. (19) along with $\partial q'/\partial t$ due to axial excitation (similar to the derivation for 1T mode). Multiplying with r^2 and integrating over the volume gives the oscillator model for the 1R mode with forcing from the 1T mode as:

$$\ddot{\eta}_2 + \alpha_2 \dot{\eta}_2 + \omega_2^2 \eta_2 = \beta_2 \dot{\eta}_2 + \sigma(\dot{\chi}_1 \eta_1 + \dot{\eta}_1 \chi_1)$$
$$= \beta_2 \dot{\eta}_2 + \sigma(\eta_1^2 + \dot{\eta}_1 \chi_1) \tag{27}$$

where, σ is the integral of $r^2\phi^2(r,\theta)$ multiplied with a coefficient. When the 1T mode reaches limit cycle, $\eta_1 = A_{1,lc} \cos(\omega_1 t + \varphi)$ and it can be shown that $\eta_1^2 + \dot{\eta}_1 \chi_1 = A_{1,lc}^2 \cos(2\omega_1 t + 2\varphi)$. As the 1R oscillator is forced at frequency $2\omega_1$, η_2 can be expressed as $\Gamma e^{2i\omega_1 t}$. Replacing this in Eq. (27), we derive:

$$\Gamma = \frac{\sigma A_{1,lc}^2 e^{2i\varphi} e^{i\xi}}{[(\omega_2^2 - 4\omega_1^2)^2 + 4\omega_1^2(\alpha_2 - \beta_2)^2]^{1/2}} \tag{28}$$

where,

$$\xi = -\arctan\left(\frac{2\omega_1(\alpha_2 - \beta_2)}{\omega_2^2 - 4\omega_1^2}\right) \qquad for \ \ \omega_2 > 2\omega_1$$
$$= -\pi + \arctan\left(\frac{2\omega_1(\alpha_2 - \beta_2)}{4\omega_1^2 - \omega_2^2}\right) \quad for \ \ \omega_2 < 2\omega_1 \tag{29}$$

24

The phase of $q'_{trans,1T}$ can be derived from the phase of $\eta_1 \chi_1$. Given $\eta_1 = A_{1,lc}\ cos(\omega_1 t + \varphi)$, the phase of $q'_{trans,1T}$ and η_2 are $(2\omega_1 t + 2\varphi - \pi/2)$ and $(2\omega_1 t + 2\varphi + \xi)$, respectively. From Eq. 29, ξ tends to $-\pi/2$ close to resonance. Therefore, the phase difference between $q'_{trans,1T}$ and η_2 tends to zero and the Rayleigh index computed with $q'_{trans,1T}$ and p'_{1R} (η_2) is positive. This shows that if the overall q' for a mode contains q' driven by itself and by another mode, a positive Rayleigh index does not necessarily indicate that it is an unstable mode because this positive Rayleigh index can be due to the forcing from another mode also.

4.1.1. Time-domain oscillator simulation:

The analytical expressions derived in the previous section are validated with a time-domain simulation of the coupled oscillators. The two oscillators (Eq. (21) and (27)) are modeled in MATLAB Simulink with fourth order Runge-Kutta formulation for time-stepping. As this is a representative model, simple values for parameters can be chosen. The choice of parameters should satisfy certain conditions which are discussed in the Appendix (Supplemental material). Model parameters are as follows: $c = 1$; $R = 1$; $\beta_1 = 0.5$; $\alpha_1 = 0.4$; $\kappa_1 = 2$; $\beta_2 = 0.4$; $\alpha_2 = 0.5$; $\sigma = 0.2$.

Figures 11a and 11b show the time-domain oscillations of oscillator variables η_1 and η_2. In Fig. 11a, we observe that η_1 grows until it reaches limit cycle. For η_2, the amplitude decreases at the very beginning because this mode is linearly stable. However, once η_1 reaches sufficient amplitude, the second oscillator is forced resulting in increasing amplitude for η_2. Figure 11c shows the frequency spectrum of overall oscillation ($\eta_1 + \eta_2$). The analytical values of the limit cycle amplitudes are also marked and show very good agreement with the time-domain results. Similar to the frequency spectrum of Urbano et al. [45] (Fig. 8), Fig. 11c displays two distinct peaks with the second peak exactly at twice the frequency of the first peak. Therefore, near-resonance with the 1R mode caused by q' due to v'_{1T} can explain the high amplitude of the 1R mode even though it is linearly stable.

4.1.2. Sensitivity study

A parametric study is conducted to investigate the dependence of amplitude of the second mode on parameters β_2 and ω_2 (the eigenfrequency of the second mode). Figure 12 shows the variation of amplitude of the second peak with changing of these parameters. Here, only the second peak is shown because the first peak is not affected by changes in β_2 and ω_2. For comparison of amplitudes of the first and second peaks, the amplitude of the first peak shown in Fig. 11c (at about 0.44) should be used. By increasing β_2 up to α_2, it can be observed that the amplitude of the second peak increases as the effective damping of this mode decreases (Fig. 12a). This behavior is expected from the expression of amplitude of the 1R mode (Eq. 28), where increasing β_2 decreases $(\alpha_2 - \beta_2)$ and thus, the amplitude increases.

In Fig. 12b, ω_2 is brought closer to $2\omega_1$. In our analytical explanation of the coupling mechanism, we assumed that the mean flow in the chamber is zero and speed of sound is homogeneous. Therefore, ω_2 was shown to be at $2.081\omega_1$. However, with other mean fields or by taking longitudinal direction and injectors into consideration, ω_2 can be different, but still close to $2\omega_1$. Thus, it would be interesting to know how the amplitude of the mode changes with decreasing difference between ω_2 and $2\omega_1$. As ω_2 is brought closer to $2\omega_1$, the amplitude increases significantly. Bringing ω_2 closer to $2\omega_1$ by even 1% causes amplification of the amplitude by 1.5 times thus showing high sensitivity of the amplitude to the difference between ω_2 and $2\omega_1$.

Our study uses a cylindrical combustion chamber to explain the coupling mechanism between a dominant transverse mode and a higher order mode through flame response to transverse velocity excitation and relates it to the observation made by Urbano et al. [45] in a rocket thrust chamber. This coupling mechanism is not restricted to only a cylindrical or rocket engine combustion chamber, but is applicable to any combustion chamber with transverse modes and symmetric compact flames. For example, in an annular gas turbine, the

eigenfrequency of the second azimuthal mode is twice the frequency of the first azimuthal mode. If the first azimuthal mode is dominant, transverse velocity excitation of the flames can force the second azimuthal mode and even if the second mode is linearly stable, resonance can cause its amplification (similar to $\omega_2 = 2\omega_1$ in Fig. 12b).

5. Summary and Conclusions

In this study, the response of a symmetric, acoustically compact flame to uniform transverse velocity excitation v' was investigated. As described previously, in such a configuration heat release fluctuations q' are invariant to the direction of v' and thus the flame response is *inherently non-linear*, i.e., even for infinitesimal amplitudes the heat release response at the forcing frequency is zero and the dominant response is observed at twice the forcing frequency. This study provides a novel approach to formulate a lumped low-order model for such non-linear behavior in terms of Volterra series, which constitutes a general framework to model non-linear, time invariant, dynamical systems. We demonstrated that Volterra series comprising only even-order kernels can represent the inherently nonlinear dynamics of a flame excited by transverse velocity. This suggests that Volterra series can be a suitable framework for system identification of the flame response to v' and for modeling other kinds of non-linearity in the flame response in future investigations.

As a possible realization of a Volterra series, an ad-hoc model for the inherently nonlinear flame response to transverse excitation was proposed and validated with good success against CFD results. In its current form, this low-order model is applicable only with single-frequency forcing. Given that in thermoacoustics one often focuses on the flame response at certain frequencies, this restriction is acceptable, but nevertheless should be eliminated in future studies.

Although the flame response to v' is in general significantly weaker than the response to axial velocity excitation, frequency doubling can lead to coupling

of a dominant transverse mode with a higher order mode. At near resonance conditions, i.e., if the eigenfrequency of the higher order mode is close to twice the frequency of the dominant mode, significant amplitudes may result. This mechanism of modal coupling was put forward as an explanation of the observations of Urbano et al. [45, 46] in a small-scale thrust chamber, where a radial mode displays significant amplitude at exactly twice the frequency of an unstable transverse mode. As the eigenfrequency of the radial mode is close to twice the frequency of the unstable transverse mode, unsteady heat release q' driven by the v' field of the transverse mode causes near-resonance with the radial mode and thus the radial mode can reach significant amplitude even if it is linearly stable.

Modal coupling due to v' excitation as described in the present study for the case of a cylindrical combustion chamber may also play a role in other combustor configurations, e.g., annular combustors of gas turbines. Therefore, it is important to take into account the frequency-doubled flame response to transversal excitation. The coupled dynamics of thermoacoustic modes in combustor configurations, where the flames are perturbed simultaneously by axial and transverse velocity excitation, appears to be a worthy subject of further studies.

Acknowledgments

References

[1] D.T. Harrje, F.H. Reardon, Liquid Propellant Rocket Combustion Instability (Tech. Rep. No. NASA-SP-194). Scientific and Technical Information Office, National Aeronautics and Space Administration, Washington DC, U.S.A. (1972).

[2] F.H. Reardon, L. Crocco, D.T. Harrje, Velocity effects in transverse mode liquid propellant rocket combustion instability, AIAA J. 2 (1964) 1631-1641.

[3] L. Crocco, D.T. Harrje, F.H. Reardon, Transverse Combustion Instability in Liquid Propellant Rocket Motors, ARS J. 32 (1962) 366-373.

[4] W. Krebs, G. Walz, S. Hoffmann, Thermoacoustic Analysis of Annular Combustor, in: 5th AIAA Aeroacoustics Conference, Vol. AIAA-99-1971, Seattle, WA, 1999.

[5] J. Lepers, W. Krebs, B. Prade, P. Flohr, G. Pollarolo, A. Ferrante, Investigation of Thermoacoustic Stability Limits of an Annular Gas Turbine Combustor Test-Rig with and without Helmholtz Resonators, in: ASME Turbo Expo 2005: Power for Land, Sea, and Air, GT2005-68246. American Society of Mechanical Engineers, 2005, pp. 177-189.

[6] A.P. Dowling, S.R. Stow, Acoustic Analysis of Gas Turbine Combustors, J. Propuls. Power 19 (2003) 751-764.

[7] J. Kopitz, A. Huber, T. Sattelmayer, W. Polifke, Thermoacoustic Stability Analysis of an Annular Combustion Chamber with Acoustic Low Order Modeling and Validation Against Experiment, in: ASME Turbo Expo 2005: Power for Land, Sea, and Air, GT2005-68797, American Society of Mechanical Engineers, Reno-Tahoe, Nevada, USA, 2005, pp. 583-593.

[8] J. O'Connor, V. Acharya, T. Lieuwen, Transverse combustion instabilities: Acoustic, fluid mechanic, and flame processes, Prog. Energy Combust. Science 49 (2015) 1-39.

[9] V. Acharya, M. Malanoski, M. Aguilar, T. Lieuwen, Dynamics of a Transversely Excited Swirling, Lifted Flame: Flame Response Modeling and Comparison With Experiments, J. Eng. Gas Turb. Power 136 (2014) 051503.

[10] A. Saurabh, C.O. Paschereit, Dynamics of premixed swirl flames under the influence of transverse acoustic fluctuations, Combust. Flame 182 (2017) 298-312.

[11] W. Polifke, C.O. Paschereit, K. Döbbeling, Constructive and Destructive Interference of Acoustic and Entropy Waves in a Premixed Combustor with a Choked Exit, Int. J. Acoustics Vib. 6 (2001) 135-146.

[12] B. Pomeroy, C. Morgan, W. Anderson, Response of a Gas-Centered Swirl Coaxial Injector to Transverse Instabilities, in: 47th AIAA/ASME/SAE/ASEE Joint Propulsion Conference & Exhibit, San Diego, California, 2011.

[13] J. Blimbaum, M. Zanchetta, T. Akin, V. Acharya, J. O'Connor, D.R. Noble, T. Lieuwen, Transverse to Longitudinal Acoustic Coupling Processes in Annular Combustion Chambers, Int. J. Spray Combust. Dyn. 4 (2012) 275-298.

[14] S. Gröning, J. Hardi, D. Suslov, M. Oschwald, Injector-Driven Combustion Instabilities in a Hydrogen/Oxygen Rocket Combustor, J. Propuls. Power 32 (2016) 560-573.

[15] M.F. Heidmann, C.E. Feiler, Evaluation of Tangential Velocity Effects on Spinning Transverse Combustion Instability (Tech. Rep. No. NASA TN D-3406). National Aeronautics and Space Administration, Washington DC, U.S.A. (1966).

[16] M.F. Heidmann, P.R. Wieber, Analysis of frequency response characteristics of propellant vaporization (Tech. Rep. No. NASA-TN-D-3749). Na-

tional Aeronautics and Space Administration, Washington DC, U.S.A. (1966).

[17] S. Ducruix, C. Rey, S. Candel, A method for the transverse modulation of reactive flows with application to combustion instability, Combust. Theory Modelling 9 (2005) 5-22.

[18] V. Acharya, Shreekrishna, D.-H. Shin, T. Lieuwen, Swirl effects on harmonically excited, premixed flame kinematics, Combust. Flame 159 (2012) 1139-1150.

[19] F. Lespinasse, F. Baillot, T. Boushaki. Responses of V-flames placed in an HF transverse acoustic field from a velocity to pressure antinode, Comptes Rendus Mcanique 341 (2013) 110-120.

[20] L. Hakim, T. Schmitt, S. Ducruix, S. Candel, Dynamics of a transcritical coaxial flame under a high-frequency transverse acoustic forcing: Influence of the modulation frequency on the flame response, Combust. Flame 162 (2015) 3482-3502.

[21] M. Roa, S.A. Schumaker, D.G. Talley, High Frequency Transverse Acoustic Forcing of Cryogenic Impinging Jets at High Pressure, in: 52nd AIAA/SAE/ASEE Joint Propulsion Conference, Salt Lake City, UT, 2016.

[22] S. Beinke, F. Tonti, S. Karl, J. Hardi, M. Oschwald, B. Dally, Modelling Flame Response of a Co-axial LOx/GH2 Injection Element to High Frequency Acoustic Forcing, in: 7th European Conference for Aeronautics and Aerospace Sciences (EUCASS), 2017.

[23] C. Li, M. Zhu, J.P. Moeck, An analytical study of the flame dynamics of a transversely forced asymmetric two-dimensional Bunsen flame, Combust. Theory Modelling 21 (2017) 976-995.

[24] M. Roa, D.G. Talley, Unsteady and Transversely Forced Dynamics of Two-Phase Multi-Element Shear Coaxial Flows, in: AIAA Propulsion and Energy 2019 Forum, Indianapolis, IN, 2019.

[25] M. Roa, D.G. Talley, Acoustic Forcing and Sensitivity of the Hydrodynamic Instabilities and Flame Dynamics from Hydrogen/LOX Shear Coaxial Flames, in: AIAA Scitech 2020 Forum, Orlando, FL, 2020.

[26] G. Staffelbach, L.Y.M. Gicquel, G. Boudier, T. Poinsot, Large Eddy Simulation of self excited azimuthal modes in annular combustors, Proc. Combust. Inst. 32 (2009) 2909-2916.

[27] J.R. Dawson, N.A. Worth, Flame dynamics and unsteady heat release rate of self-excited azimuthal modes in an annular combustor, Combust. Flame 161 (2014) 2565-2578.

[28] B. Knapp, Z. Farago, M. Oschwald, Interaction of LOX/GH2 Spray-Combustion with Acoustics, in: 45th AIAA Aerospace Sciences Meeting and Exhibit, Reno, Nevada, 2007.

[29] A. Saurabh, C. Paschereit, Premixed Flame Dynamics in Response to Two- Dimensional Acoustic Forcing, Combust. Science and Technology 191 (2019) 1184-1200.

[30] B. Knapp, M. Oschwald, High Speed Visualization of Flame Response in a LOx/H2 Combustion Chamber During External Excitation, in: 12th International Symposium on Flow Visualization, Göttingen, Germany, 2006.

[31] B. Pomeroy, N. Nugent, W.E. Anderson, Measuring Transverse Combustion Stability at Full Scale Frequencies in a Subscale Combustor, in: 46th AIAA/ASME/SAE/ASEE Joint Propulsion Conference & Exhibit, 2010.

[32] M. Zellhuber, L. Tay-Wo-Chong, W. Polifke, Non-Linear Flame Response at Small Perturbation Amplitudes – Consequences for Analysis of Thermoacoustic Instabilities, in: Proceedings of the European Combustion Meeting 2011, Cardiff, UK, 2011.

[33] M. Schmid, T. Sattelmayer, Influence of pressure and velocity perturbations on the heat release fluctuations for coaxial GH2/GO2 injection, in: 4th

European Conference for Aerospace Sciences (EUCASS), Saint Petersburg, Russia, 2011.

[34] M.F. Heidmann, P.R. Wieber, Analysis of n-Heptane vaporization in unstable combustor with traveling transverse oscillations (Tech. Rep. No. NASA TN D-3424). National Aeronautics and Space Administration, Washington DC, U.S.A. (1966).

[35] J. Hardi, M. Oschwald, B. Dally, Flame response to acoustic excitation in a rectangular rocket combustor with LOx/H2 propellants, CEAS Space J. 2 (2011) 41-49.

[36] L. Hakim, A. Ruiz, T. Schmitt, M. Boileau, G. Staffelbach, S. Ducruix, B. Cuenot, S. Candel, Large eddy simulations of multiple transcritical coaxial flames submitted to a high-frequency transverse acoustic modulation, Proc. Combust. Inst. 35 (2015) 1461-1468.

[37] P.P. Popov, W.A. Sirignano, Transverse Combustion Instability in a Rectangular Rocket Motor, J. Propuls. Power 32 (2016) 620-627

[38] A. Yang, B. Li, Y. Yan, S. Xue, L. Zhou, Experimental of combustion instability in NTO/MMH impinging combustion chambers, Chin. J. Aeronautics 33 (2020) 1476-1485.

[39] L. Crocco, D.T. Harrje, W.A. Sirignano, F.V. Bracco, J.B. Elgin, R.M. Llyod, P.K. Tang, T.S. Tonon, A.K. Varma, J.S. Wood, G.F. Zaic, Nonlinear aspects of combustion instability in liquid propellant rocket motors (No. NASA CR 72426), 1968.

[40] L. Crocco, Research on combustion instability in liquid propellant rockets, Symp. (Int.) Combust. 12 (1969) 85-99.

[41] M. Sliphorst, B. Knapp, S. Gröning, M. Oschwald, Combustion Instability-Coupling Mechanisms Between Liquid Oxygen/Methane Spray Flames and Acoustics, J. Propuls. Power 28 (2012) 1339-1350.

[42] G. Ghirardo, M.P. Juniper, Azimuthal instabilities in annular combustors: standing and spinning modes, Proc. of the Royal Society A: Mathematical, Physical and Engineering Science 469 (2013) 20130232.

[43] M. Haeringer, M. Merk, W. Polifke, Inclusion of higher Harmonics in the Flame Describing Function for Predicting Limit Cycles of self-excited Combustion Instabilitites, Proc. Combust. Inst. 37 (2018) 5255-5262.

[44] F. Selimefendigil, W. Polifke, A nonlinear frequency domain model for limit cycles in thermoacoustic systems with modal coupling, Int. J. Spray Comb. Dyn. 3 (2011) 303-330.

[45] A. Urbano, L. Selle, G. Staffelbach, B. Cuenot, T. Schmitt, S. Ducruix, S. Candel, Exploration of Combustion Instability Triggering Using Large Eddy Simulation of a Multiple Injector Liquid Rocket Engine, Combust. Flame 169 (2016) 129-140.

[46] A. Urbano, Q. Douasbin, L. Selle, G. Staffelbach, B. Cuenot, T. Schmitt, S. Ducruix, S. Candel, Study of flame response to transverse acoustic modes from the LES of a 42-injector rocket engine, Proc. Combust. Inst. 36 (2017) 2633-2639.

[47] S. Gröning, D. Suslov, M. Oschwald, T. Sattelmayer, Stability behaviour of a cylindrical rocket engine combustion chamber operated with liquid hydrogen and liquid oxygen, in: 5th European Conference for Aeronautics and Space Sciences EUCASS 2013, Proceedings 5th EUCASS, 2013.

[48] S. Gröning, J. Hardi, D. Suslov, M. Oschwald, Influence of hydrogen temperature on the stability of a rocket engine combustor operated with hydrogen and oxygen: A new hydrogen temperature ramping experiment, CEAS Space J. 9 (2017) 59-76.

[49] S. Gröning, Untersuchung selbsterregter Verbrennungsinstabilitten in einer Raketenbrennkammer, Ph.D. Thesis, RWTH Aachen (2017).

[50] A. Urbano, L. Selle, Driving and damping mechanisms for transverse combustion instabilities in liquid rocket engines, J. Fluid Mech. 820 (2017) R2.

[51] W. Van Drongelen, Signal processing for neuroscientists, 2nd Edition, Academic Press, London, 2018.

[52] F. Selimefendigil, Identification and Analysis of Nonlinear Heat Sources in Thermo-Acoustic Systems, Doctoral Thesis, TU München, 2010.

[53] W. Polifke, C.J. Lawn, On the Low-Frequency Limit of Flame Transfer Functions, Combust. Flame 151 (2007) 437-451.

[54] L. Crocco, S.I. Cheng, Theory of Combustion Instability in Liquid Propellant Rocket Motors, no. 8 in AGARDograph. Butterworths Science Publications, New York, 1956.

[55] N. Noiray, M. Bothien, B. Schuermans, Investigation of azimuthal staging concepts in annular gas turbines, Combust. Theory Modelling 15 (2011) 585-606.

[56] G. Bonciolini, Modelling of Thermoacoustic Dynamics in Gas Turbines Applications, Doctoral Thesis, ETH Zürich, Zürich, Switzerland, 2019.

[57] V.N. Kornilov, R. Rook, J.H.M. ten Thije Boonkkamp, L.P.H. de Goey, Experimental and Numerical Investigation of the Acoustic Response of Multi-Slit Bunsen Burners, Combust. Flame 156 (2009) 1957-1970.

[58] S. Jaensch, M. Merk, E.A. Gopalakrishnan, S. Bomberg, T. Emmert, R.I. Sujith, W. Polifke, Hybrid CFD/Low-Order Modeling of Nonlinear Thermoacoustic Oscillations, Proc. Combust. Inst. 36 (2017) 3827-3834.

[59] A. Avdonin, M. Meindl, W. Polifke, Thermoacoustic analysis of a laminar premixed flame using a linearized reacting flow solver, Proc. Combust. Inst. 37 (2019) 5307-5314.

[60] V. Sharifi, A.M. Kempf, C. Beck, Large-Eddy Simulation of Acoustic Flame Response to High-Frequency Transverse Excitations, AIAA J. 57 (2019) 1-14.

[61] M. Schulze, T. Sattelmayer, Eigenvalue Analysis for the Prediction of Initial Growth Rates of Thermoacoustic Instability in Rocket Motors, in: 53rd AIAA Aerospace Sciences Meeting, American Institute of Aeronautics and Astronautics, Kissimmee, Florida, USA, 2015.
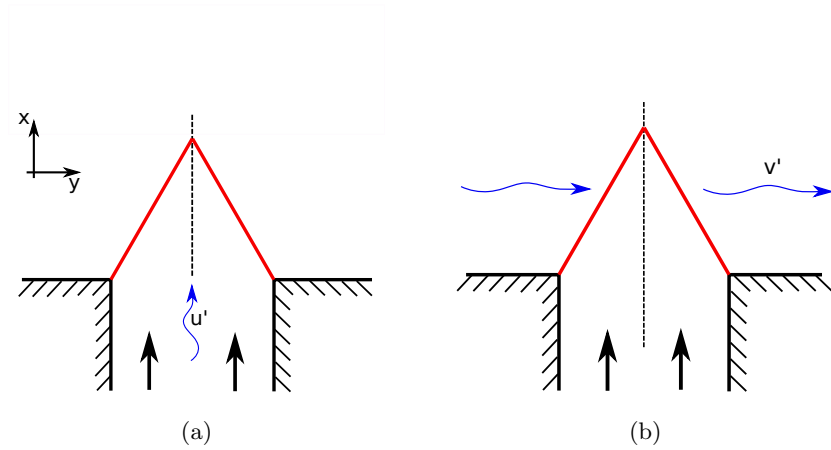
Figure 1: Excitation of a compact symmetric flame at (a) a pressure anti-node (v' node) and (b) a pressure node (v' anti-node). The flame (mean shape represented by red lines) is anchored at the flame holder (outline with black shaded lines). Dashed vertical black lines along the flame center indicate the symmetry line. Bold black arrows depict the mean flow of fuel and oxidizer. Wavy arrows depict the direction of velocity fluctuation at an instant (wavy shape of arrow does not represent wavelength). Axial velocity fluctuation u' is induced due to pressure oscillation p', which is strongest at the p' anti-node.
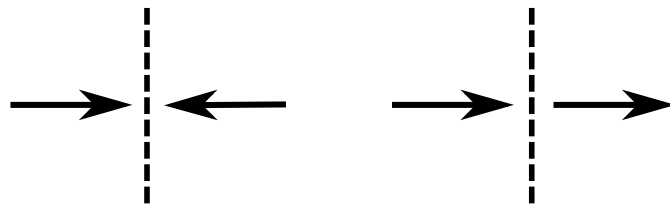
Figure 2: Example to demonstrate reflection-symmetric (left) and reflection-anti-symmetric (right) vector field about centre axis $y = 0$ (dashed lines).
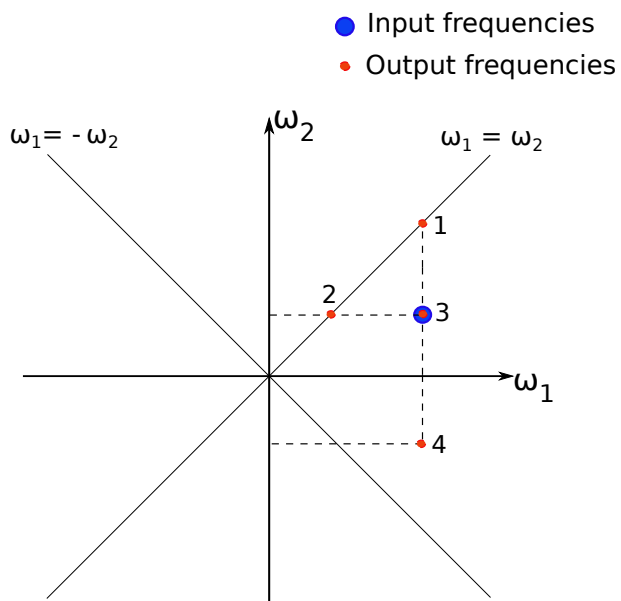
Figure 3: 2D mapping of the second-order transfer function ψ at input frequencies along ω_1 and ω_2 axes (denoted by the blue dot). The red dots signify the output frequencies at - (1) $2\omega_1$, (2) $2\omega_2$, (3) $\omega_1 + \omega_2$ and (4) $\omega_1 - \omega_2$.
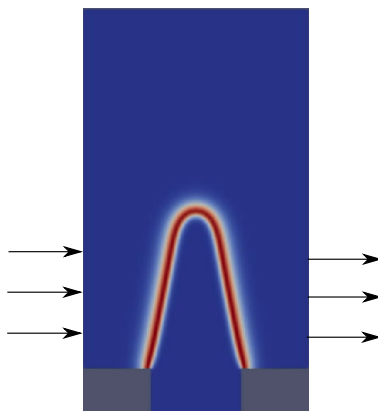
Figure 4: 2D symmetric flame setup for CFD. Arrows depict v' forcing at a time instance.
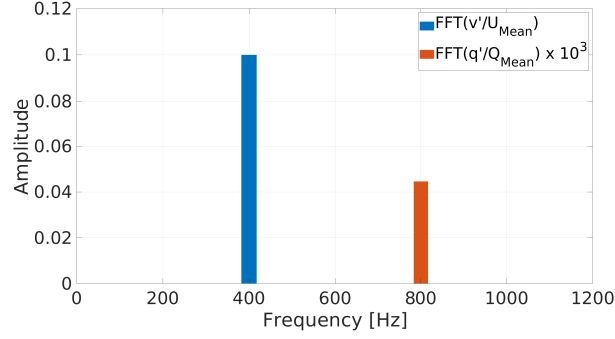
Figure 5: Frequency spectrum of v' (blue) and q' (red) at forcing frequency of 400 Hz at 10% forcing, i.e., the amplitude of v' is 10% of the axial mean velocity U_{Mean}. Note: The FFT of q' has been scaled with a factor of 10^3.
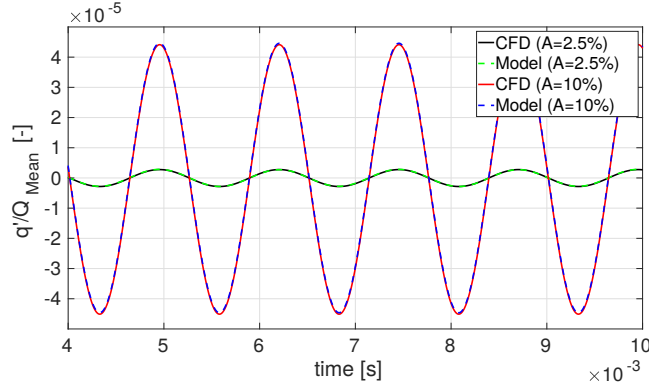
Figure 6: $q'(t)$ from CFD with two amplitudes of v' : 2.5% (solid black line) and 10% (solid red line) of the axial mean velocity. Amplitudes of normalized q' (Eq. (13)) at 2.5% and 10% forcing are 2.76×10^{-6} and 4.40×10^{-5} respectively. Outputs from the ad-hoc model shown in dashed lines (green and blue for 2.5% and 10% forcing, respectively) are with same k and τ for both amplitudes. The values of parameters for this frequency are : $k = 3.5 \times 10^{-6}$ and $\tau = 8.9 \times 10^{-4}s$.

39
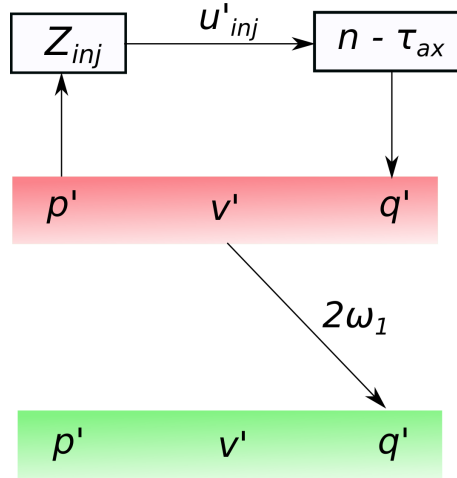
Figure 7: A transverse mode (red, top) with eigenfrequency ω_1 is unstable due to the thermoacoustic feedback through axial velocity perturbation at injector exit u'_{inj} induced by p' of this mode. The flame response to u'_{inj} is governed by a flame model (for example, $n - \tau_{ax}$ model). A higher order mode (green, bottom) with eigenfrequency $\omega_2 \approx 2\omega_1$ is stable and thus, thermoacoustic feedback is not significant for this mode. Frequency-doubled flame response to transverse velocity fluctuation v' of the unstable mode causes forcing of the stable mode.
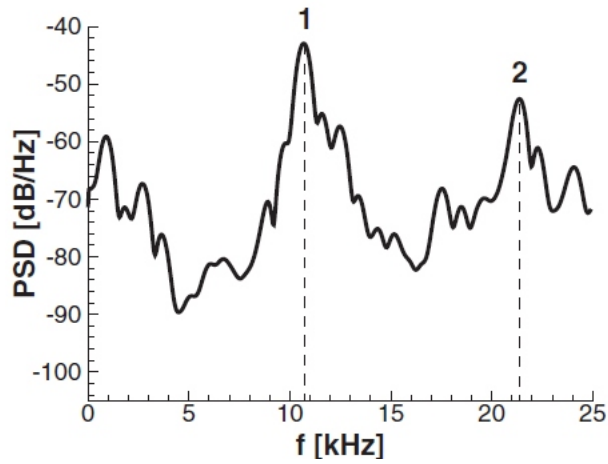
Figure 8: PSD of pressure perturbation from the LES of a small-scale rocket thrust chamber reproduced from ref. [45].
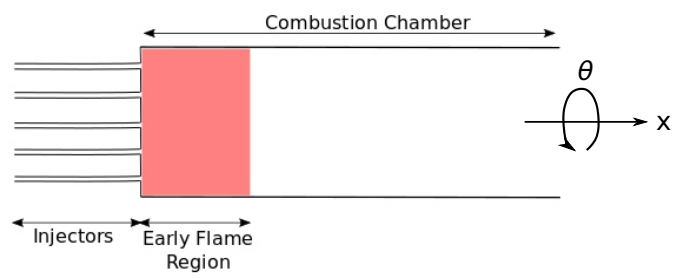
Figure 9: Schematic of the meridional cross-section of the cylindrical combustion chamber of a rocket thrust chamber with region of interest shown as the early flame region.
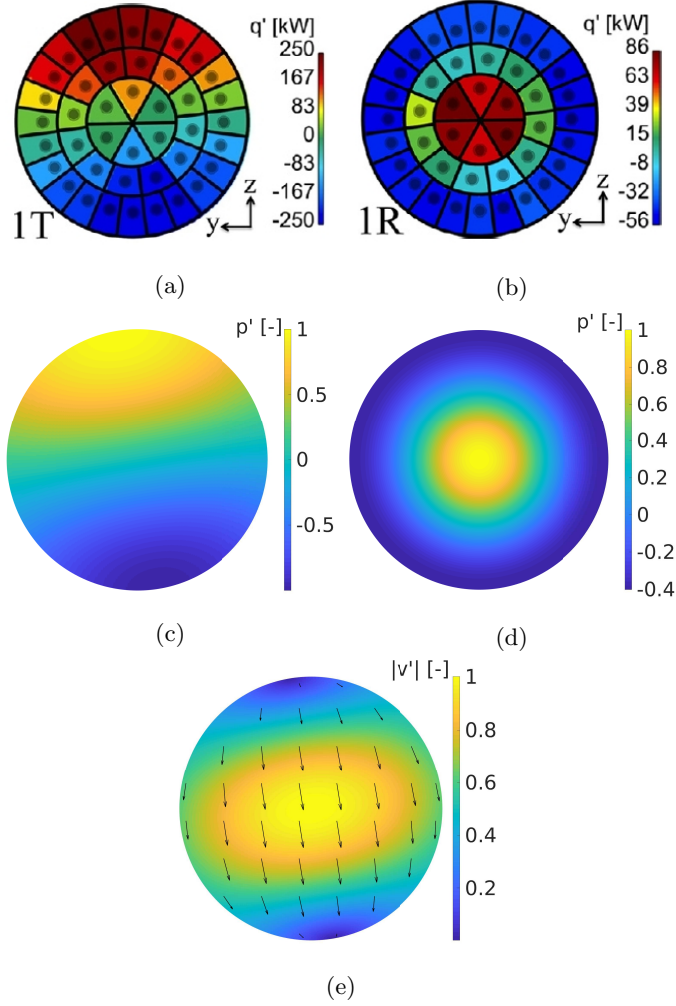
Figure 10: Local spatial integrated heat release around each flame for (a) 1T mode and (b) 1R mode reproduced from ref. [46]. Spatial distribution of (c) $\hat{p}'$ from 1T mode, (d) $\hat{p}'$ from 1R mode, (e) $|\hat{v}'| = \sqrt{\hat{v_r'}^2 + \hat{v_\theta'}^2}$ from 1T mode according to Eq. (16). Distribution has been normalized with the respective maximum value for (c)-(e). Arrows in (e) depict direction of transverse velocity at a time instance. The orientation of 1T mode in (c) and (e) is adjusted to match the orientation in (a).
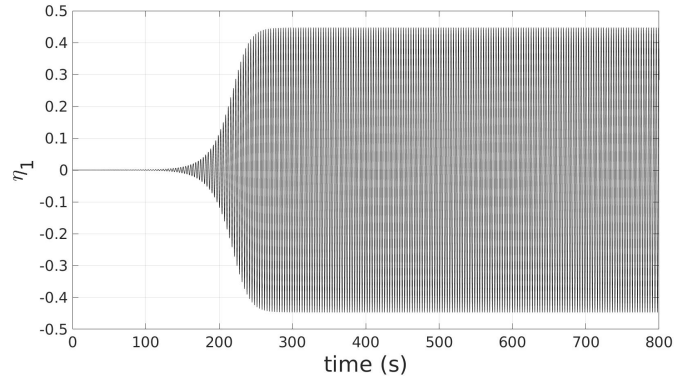
(a)
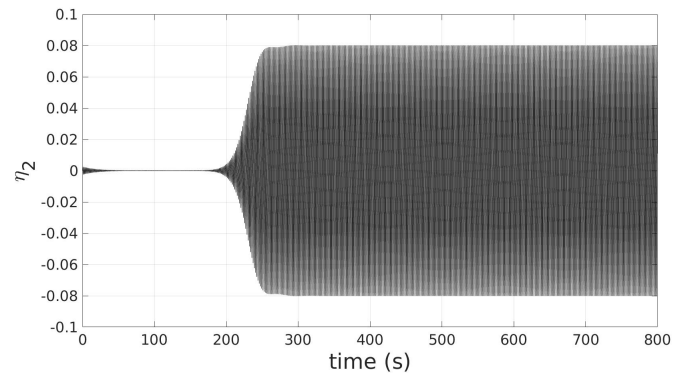
(b)
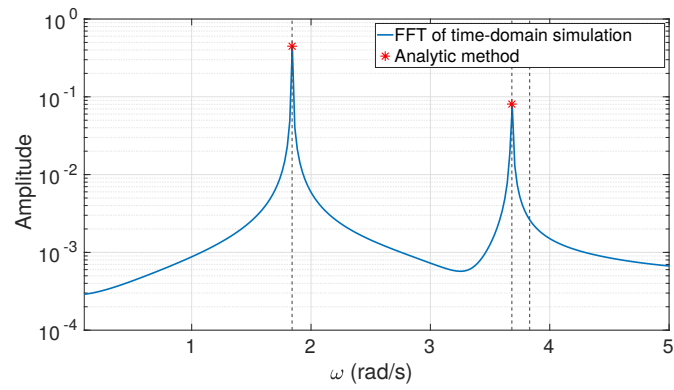
(c)

Figure 11: Time evolution of (a) η_1 and (b) η_2. (c) Frequency spectrum of $\eta_1 + \eta_2$ showing a second peak at twice the frequency of the first peak. Red crosses denote the limit cycle amplitudes of two frequencies calculated analytically from Eq. (22) and (28). Three dashed lines in (c) denote the frequencies at ω_1, $2\omega_1$, and ω_2 from left to right.

43
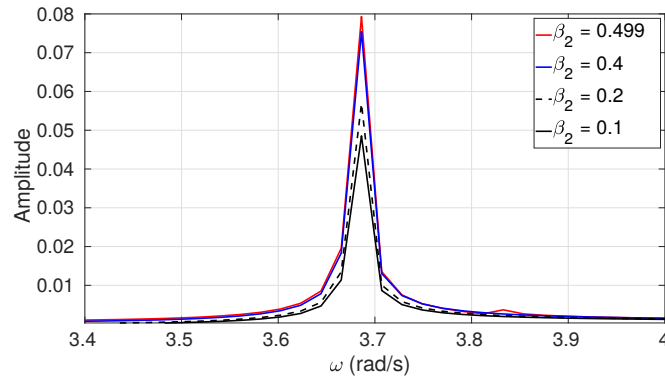
(a) $\alpha_2 = 0.5, \sigma = 0.2$
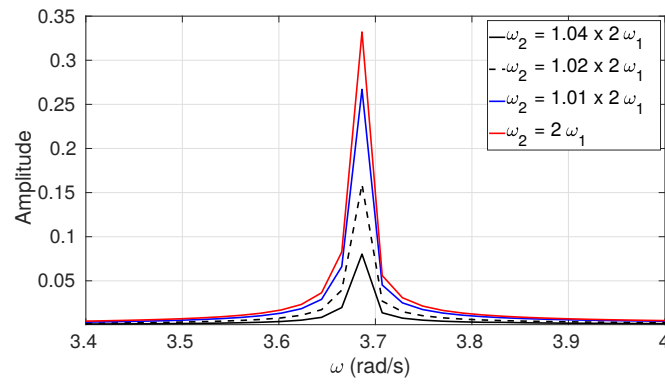
(b) $\beta_2 = 0.49, \alpha_2 = 0.5$

Figure 12: The amplitude of second peak with changing (a) β_2 (coefficient of flame response to u' excitation for the 1R mode), (b) ω_2 (the eigenfrequency of the second mode).